Reprinted from June 1992, Vol. 114, Part 2, Journal of Applied Mechanics

Differential Hardening in Sheet Metal Under Biaxial Loading: A Theoretical Framework

R. Hill
Department of Applied Mathematics and Theoretical Physics, University of Cambridge, Cambridge CB3 9EW, England

J. W. Hutchinson
Division of Applied Sciences, Harvard University, Cambridge, MA 02138
Fellow ASME

A simple constitutive framework is proposed to take account of progressive changes in a stress-based criterion of yielding as plastic deformation accumulates. The analysis is relevant to a sheet of isotropic or orthotropic material which is subsequently loaded in its plane by biaxial tensions (σ_1, σ_2) *in arbitrary fixed ratio. Under these circumstances there is evidence that texture development causes significant changes in the shapes of successive yield loci in* (σ_1, σ_2) *space. Here such departures from geometric similarity are explicitly linked to a presumed dependence on* σ_1/σ_2 *of the exponent* m *in a standard power-law representation of the stress-strain characteristic under each constant value of* σ_1/σ_2. *The linkage is formulated in detail for several types of representation, and it is shown how a family of yield loci associated with any conjectural dependence* $\mathrm{m}(\sigma_1/\sigma_2)$ *can be generated readily by computer graphics. Some typical examples are given, in particular when* $\mathrm{m}(\sigma_1/\sigma_2)$ *reflects the distinctive trends reported for certain kinds of brass and aluminum sheet (e.g., Wagoner, 1980; Stout and Hecker 1983).*

1 Objectives

The context is elastoplastic response of a textured sheet of polycrystalline material under in-plane biaxial loads. In its as-received condition the material is assumed to be orthotropic at a macroscopic level. Uniform tensions in arbitrary fixed ratios are applied parallel to the orthotropic axes, which hence remain embedded in the material as it deforms. The aim of the analysis is a constitutive framework that accommodates differential hardening due to textural changes accompanying plastic deformation. The approach is macroscopic and phenomenological only: we attempt no correlation with statistics at the level of crystal geometries, orientations, slip systems, or Schmid stresses (e.g., Lequeu and Jonas, 1988; Chan and Lee, 1990).

2 General Framework

A typical yield locus in the cartesian space of the principal Cauchy stresses (σ_1, σ_2) will be expressed in polar coordinates:

$$\phi(\tau,\theta) = \sigma \tag{1}$$

where $(\sigma_1,\sigma_2) = \tau(\cos\theta, \sin\theta)$ as shown in Fig. 1 and $0 \le \theta \le 2\pi$. The function ϕ is here normalized by the current yield stress σ in equibiaxial tension, which means that $\phi(\sqrt{2}\sigma, 1/4\pi) \equiv \sigma$. Regarding the conceptual status of yield loci, it is recalled that any particular one is the product of a *specific* loading path. Moreover, its geometry and scale necessarily reflect the terminal texture generated by the associated strain history, which is likewise specific for that locus.

In principle, then, if the same terminus in stress space were to be approached by some other route, the strain history and final texture would both differ. So therefore would the resulting locus, in greater or lesser degree according to the circumstances. Since the nature of this latter type of path dependence has been little explored, we ignore it. In so doing, we follow custom and idealize the totality of yield loci attainable from a given initial state as a *non-intersecting* and *singly infinite* family. Its members are not required to be self-similar, however, as in classical formulations where function $\phi(\tau,\theta)$ reduces to $\tau\phi(\theta)$ simply. On the contrary, progressive changes

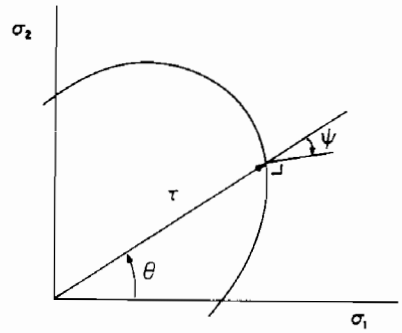

Fig. 1 Typical yield locus in (σ_1,σ_2) space, showing polar coordinates (τ,θ) and the clockwise angle ψ between a radius and the local outward normal

Contributed by the Applied Mechanics Division of THE AMERICAN SOCIETY OF MECHANICAL ENGINEERS for presentation at the 1992 ASME Summer Mechanics and Materials Meeting, Tempe, AZ, Apr. 28-May 1, 1992.

Discussion on this paper should be addressed to the Technical Editor, Prof. Leon M. Keer, The Technological Institute, Northwestern University, Evanston, IL 60208, and will be accepted until four months after final publication of the paper itself in the JOURNAL OF APPLIED MECHANICS. Manuscript received by the ASME Applied Mechanics Division, Apr. 12, 1991; final revision, Sept. 25, 1991.

Paper No. 92-APM-17.

in shape within a family are of paramount concern: we see them as inevitable concomitants of textural development during deformation.

Henceforward we focus on radial paths since these predominate in experiments on in-plane plastic response. Let γ be conjugate to τ in that

$$dw = \tau d\gamma \quad \text{at fixed } \theta \tag{2}$$

where w is the total work expended per unit volume and γ is reckoned from the origin. Generally,

$$dw = \sigma_1 d\epsilon_1 + \sigma_2 d\epsilon_2 \tag{3}$$

in terms of the logarithmic strains (ϵ_1, ϵ_2) parallel to the orthotropic axes, so the work conjugate is identifiable as

$$\gamma = \epsilon_1 \cos\theta + \epsilon_2 \sin\theta. \tag{4}$$

It is noted in passing that

$$\tau\gamma = \sigma_1\epsilon_1 + \sigma_2\epsilon_2. \tag{5}$$

Elasticity being neglected, the relation between τ and γ can be regarded as the stress versus plastic strain characteristic in a test at fixed θ. More suited to our purpose, however, is the corresponding relation between τ and w, say

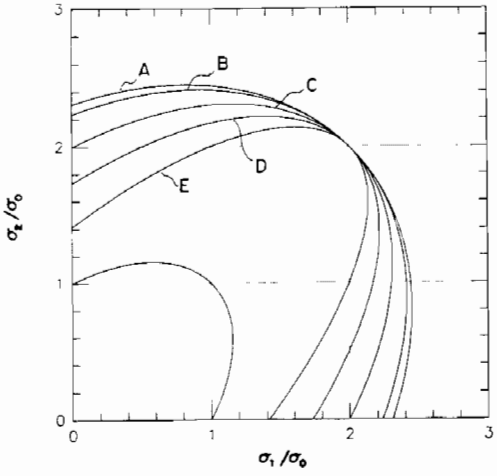

Fig. 2(*a*)

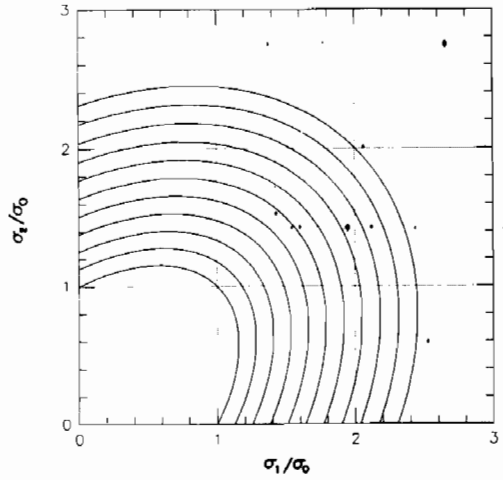

Fig. 3(*a*)

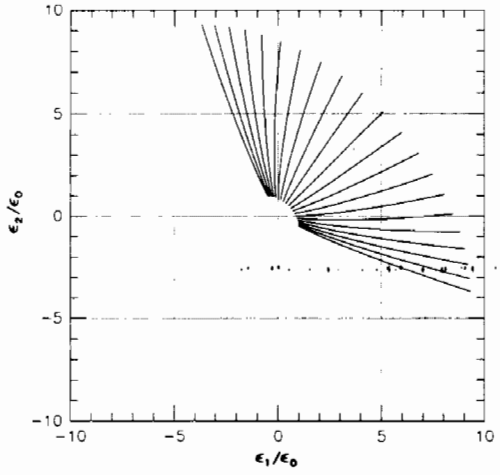

Fig. 3(*b*)

Fig. 3(*a*) Family of loci between $\tau_0(\theta)$ and $\tau_\infty(\theta)$ for case A of Fig. 2; (*b*) strain trajectories for radial stress loading with θ in the range $(0,\pi/2)$

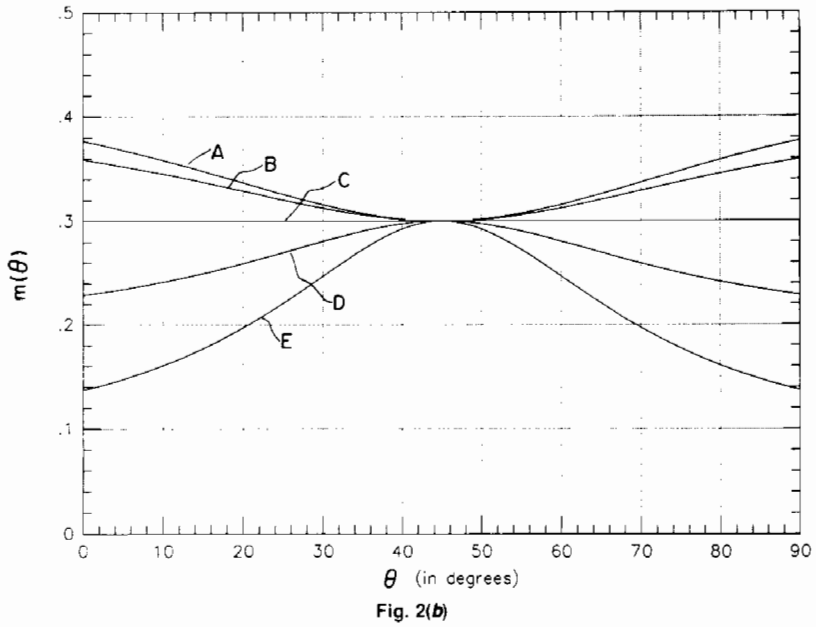

Fig. 2(*b*)

Fig. 2 The relationship between $m(\theta)$ and the outer prescribed locus $\tau_\infty(\theta)$ for $n = 0.3$ and $\sigma_\infty/\sigma_0 = 2$. The five outer loci are ellipses specified in the text. The inner locus is the Mises ellipse.

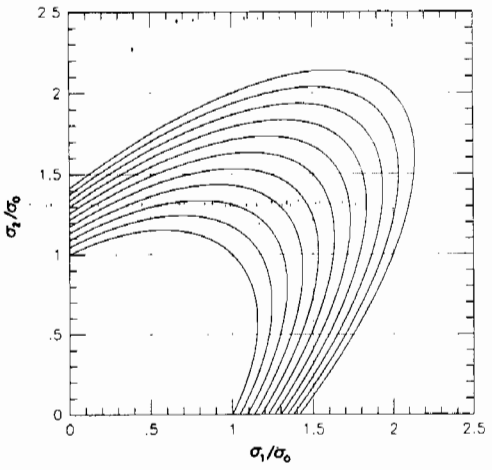

Fig. 4(a)

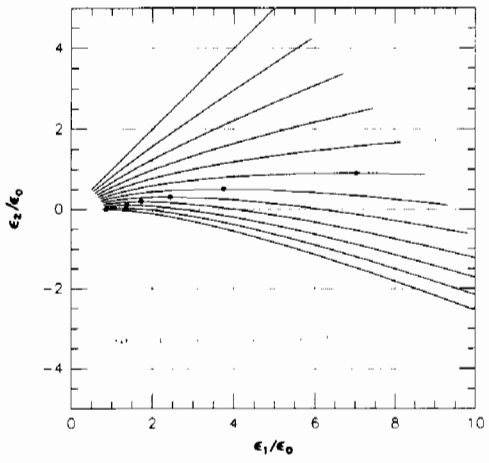

Fig. 4(b)

Fig. 4(a) Family of loci between $\tau_0(\theta)$ and $\tau_\infty(\theta)$ for case E of Fig. 2; (b) strain trajectories for radial stress loading with θ in the range $(\theta^*, \pi/4)$ where $\theta^* = \tan^{-1}(1/2)$

$$f(\tau,\theta) = w. \tag{6}$$

In particular this is

$$f\left(\sqrt{2}\sigma, \frac{1}{4}\pi\right) = w \tag{7}$$

in equibiaxial tension. Let ϵ be conjugate to σ in that

$$dw = \sigma d\epsilon \quad \text{when} \quad \theta = \frac{1}{4}\pi. \tag{8}$$

Then

$$\epsilon = \sqrt{2}\gamma = \epsilon_1 + \epsilon_2 = -\epsilon_3 \tag{9}$$

where ϵ_3 is the through-thickness logarithmic strain (the material being incompressible).

We wish to construct a family of yield loci from the radial test data. For that purpose it is hypothesized that the same amount of work per unit volume is expended on every ray to a given locus. Then the family can be parameterized by w just as well as by σ. From this standpoint the assemblage (6) of radial test data (namely $\tau(w)$ at any fixed θ) also generates the individual loci (namely $\tau(\theta)$ at any fixed w). The equivalent parameterization by σ is obtained by combining (6) and (7) as

$$f(\tau,\theta) = f\left(\sqrt{2}\sigma, \frac{1}{4}\pi\right) \tag{10}$$

which can be reduced to (1). Conversely, when a family of loci in stress space is given, it is automatically parameterized by values of σ known from intersections with the equibiaxial ray $\theta = \pi/4$. If, in addition, we assign the $\sigma(w)$ characteristic on $\theta = \pi/4$, the parameterization (6) is induced from (1), and hence the test data $\tau(w)$ at any fixed θ. Equivalently, $\sigma(\epsilon)$ for $\theta = \pi/4$ generates $\tau(\gamma)$ for any θ when the loci are given.

The proposed framework and its complementary aspects are now explained further by means of particular examples.

3 Particular Frameworks

Analytical representations of experimental stress-strain data on radial paths are often sought within a class of so-called power laws. In the present variables these laws are of type

$$\tau(\gamma,\theta) = \kappa(\theta)\gamma^{m(\theta)} \tag{11}$$

where $0 < m < 1$. There is evidence indicating that the scale factor κ and the exponent m depend on the path direction θ in at least some materials (e.g., Ghosh and Backofen, 1973; Ghosh, 1978; Wagoner, 1980, 1982; Stout and Hecker, 1983; Stout and Staudhammer, 1984). In the expectation that these dependences will be found more widely, both are allowed for in the formula. The associated increment in work along a radial path is given variously by

$$dw = \tau d\gamma = \gamma d\tau/m = d(\tau\gamma)/(1+m) \tag{12}$$

per unit volume, where for brevity the possible dependence on θ is not shown explicitly.

Empirical representations by power laws, however, are usually sufficiently accurate only above a certain threshold of strain. In order to take account of this limitation we replace (11) by

$$\tau(\gamma,\theta) = \kappa(\theta)\gamma^{m(\theta)} \quad \text{if and only if} \quad \kappa(\theta)\gamma^{m(\theta)} \geq \tau_0(\theta). \tag{13}$$

Here, $\tau_0(\theta)$ is an inner reference locus and is presumed to be attained by the expenditure of work w_0 on a radial path from the as-received state. The intervening stress-strain behavior is not represented by this formula, nor is there need of any other. Instead it is supposed merely that $\tau_0(\theta)$ and w_0 are chosen empirically in the course of fitting (13) to data over a range of strain such that $\gamma \geq \gamma_0(\theta)$, say. Then a formula corresponding to (6) for the work w on radial paths from the origin is

$$(1+m)(w-w_0)/\kappa = (\tau/\kappa)^{(1+m)/m} - (\tau_0/\kappa)^{(1+m)/m}. \tag{14}$$

Subsequent loci parameterized by values of $w > w_0$ are thus given by

$$(\tau/\tau_0)^{(1+m)/m} - 1 = (1+m)(w-w_0)/\tau_0\gamma_0. \tag{15}$$

Here

$$\tau_0 = \kappa\gamma_0^m \quad \text{but} \quad w_0 \neq \tau_0\gamma_0/(1+m) \tag{16}$$

in general, since (12) does not apply when $\gamma < \gamma_0(\theta)$. As an illustration the computations will be simplified by taking $\tau_0(\theta)\gamma_0(\theta)$ to be constant (which would be the case if, for instance, the loci within $\tau_0(\theta)$ were geometrically similar to it). Then the exterior family is generated parametrically by

$$\{(\tau/\tau_0)^{(1+m)/m} - 1\}/(1+m) = \text{constant} \tag{17}$$

on each locus. Another possibility worth considering is uniform $\tau_0(\theta)\gamma_0(\theta)/\{1+m(\theta)\}$. The exterior family is now generated by

$$(\tau/\tau_0)^{(1+m)/m} = \text{constant} \tag{18}$$

on each locus.

An alternative representation of radial stress-strain data, more suitable for certain materials, is

$$\tau = \kappa(\gamma+\eta)^m \tag{19}$$

for any range of strain. Here the material constants m, κ, and $\eta(>0)$ may all depend on θ. In the as-received state the yield locus is $\tau = \xi(\theta)$ where

$$\xi = \kappa\eta^m. \tag{20}$$

The initial rate of hardening is $d\tau/d\gamma = m\xi/\eta$, which suggests that η will usually be less than m in practice. The work on radial paths from the origin is now such that

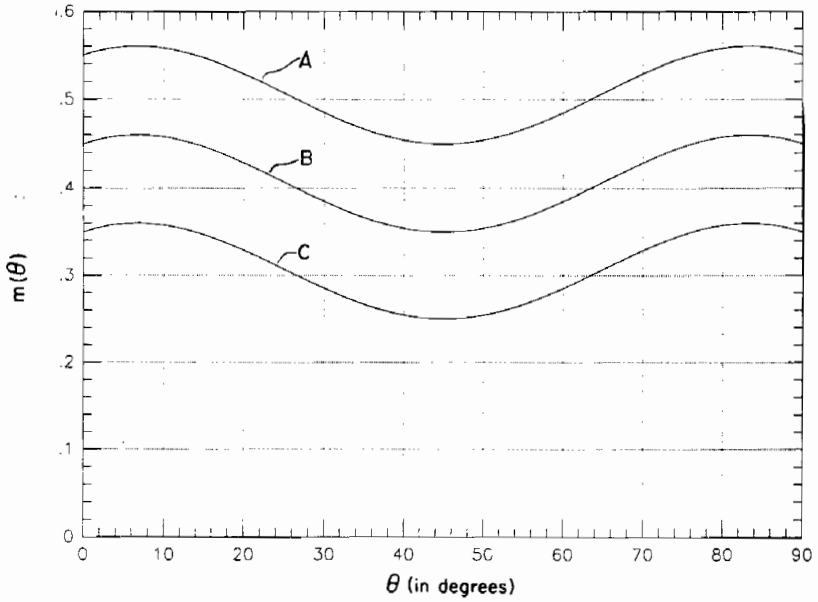

Fig. 5(a)

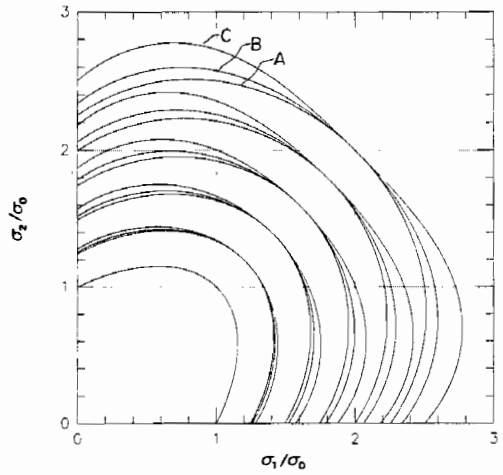

Fig. 5(b)

Fig. 5 Yield loci associated with inner Mises ellipse, $\tau_0(\theta)$, and variations of $m(\theta)$ prescribed by Eqs. (39) and (40)

$$(1+m)\,w/\kappa = (\tau/\kappa)^{(1+m)/m} - (\xi/\kappa)^{(1+m)/m} \tag{21}$$

where $\tau > \xi$. Subsequent loci parameterized by positive values of w are given by

$$(\tau/\xi)^{(1+m)/m} - 1 = (1+m)\,w/\xi\eta \tag{22}$$

in terms of assigned functions $m(\theta)$, $\xi(\theta)$, and $\eta(\theta)$. If $\xi(\theta)\eta(\theta)$ were constant, for example, then

$$\{(\tau/\xi)^{(1+m)/m} - 1\}/(1+m) = \text{constant} \tag{23}$$

on each locus, which is formally analogous to (17).

In these examples the differential hardening relative to $\tau_0(\theta)$ or $\xi_0(\theta)$ is governed solely by the dependence of exponent m on direction θ. It is this alone that determines how the ratios $\tau(\theta)/\tau_0(\theta)$ and $\tau(\theta)/\xi(\theta)$ vary over each yield locus for any given value of σ/σ_0 (the family being now regarded as parameterized by the equibiaxial tension σ). From that standpoint, explicit formulae for the relative hardening associated with (17) and (18) are

$$\{\tau(\theta)/\tau_0(\theta)\}^{[1+m(\theta)]/m(\theta)} = 1 + \left[\frac{1+m(\theta)}{1+n}\right]\{(\sigma/\sigma_0)^{(1+n)/n} - 1\}, \tag{24}$$

$$\{\tau(\theta)/\tau_0(\theta)\}^{n/(1+n)} = (\sigma/\sigma_0)^{m(\theta)/[1+m(\theta)]} \tag{25}$$

respectively, where $n = m(1/4\pi)$ and $\sqrt{2}\,\sigma_0 = \tau_0(1/4\pi)$. Similarly a replacement of (23) is available in terms of n and $\xi(\pi/4)$.

If loci generated in this fashion are always to be convex, regardless of the nature and degree of the textural changes, then admissible variations of m with θ must be constrained rather narrowly. The needed restrictions are not easily formulated, however, and so the overall outcome of any a priori selection of $m(\theta)$ tends to be unpredictable, even over quite modest ranges of σ/σ_0. At an early stage in the investigation this caused us to adopt an alternative strategy. Instead of $m(\theta)$ an outer locus, $\tau_\infty(\theta)$ say, was chosen together with the inner one, $\tau_0(\theta)$. When both are convex, so are all loci in the annulus between them (but not necessarily elsewhere). The function $m(\theta)$ is then determined by solving an equation such as (24) or (25) with n given and $\tau(\theta)$ equal to $\tau_\infty(\theta)$ (correspondingly σ equal to σ_∞). As to the status of an outer curve, it could be an empirical limit to representation by a power law; or it could be a conjectural cut-off associated with saturation hardening; or it could merely be an unexceptional locus marking an arbitrary limit to the computations.

4 Strain Paths Under Prescribed Loadings

The classical normality rule is adopted as the basis for calculating cumulative strains (ϵ_1,ϵ_2) along any path in (σ_1,σ_2) space. The direction of an outward normal to any yield locus is specified by its clockwise orientation ψ to the local radius vector, as in Fig. 1. This angle is obtainable conveniently from

$$\tan\psi = d\tau/\tau d\theta \tag{26}$$

evaluated at fixed σ in (1) or at fixed w in (6), whichever is the preferred parameterization. The anticlockwise orientation of a normal to the σ_1 coordinate axis is calculable as $\theta - \psi$, and then the incremental components of strain as

$$\frac{d\epsilon_1}{\cos(\theta-\psi)} = \frac{d\epsilon_2}{\sin(\theta-\psi)} = \frac{\sigma d\epsilon}{\sigma_1\cos(\theta-\psi) + \sigma_2\sin(\theta-\psi)} \tag{27}$$

having regard to (3) and (8). This pair of relations can be integrated straightforwardly along any path segment traversing a considered family. The only test data involved directly is that for equibiaxial tension, namely $\epsilon(\sigma)$ or $w(\sigma)$; the rest is accounted for already in the particular geometry.

Various aspects of the general correspondence between paths

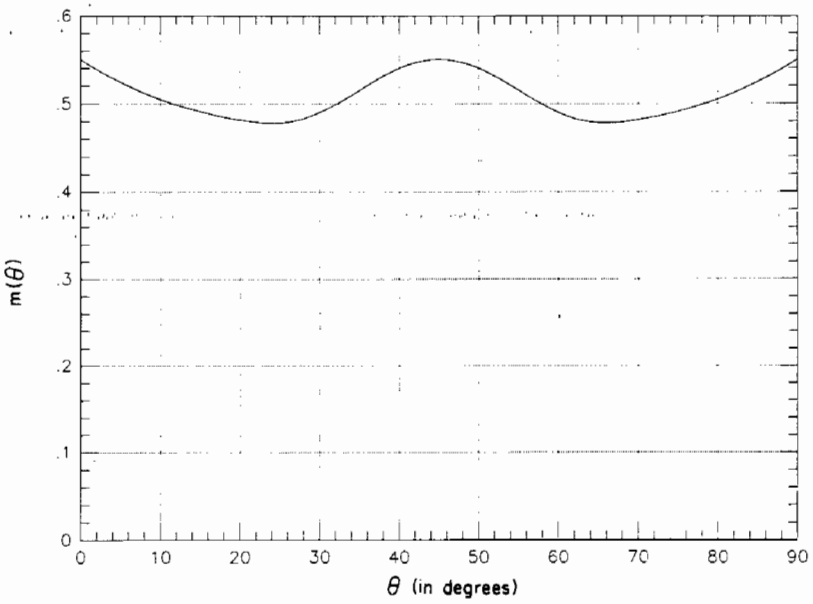

Fig. 6(a)

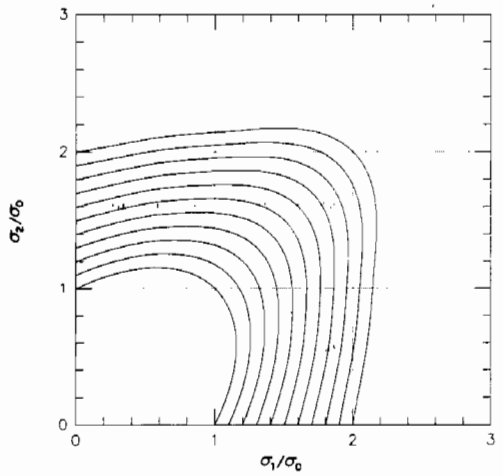

Fig. 6(b)

Fig. 6 Yield loci associated with inner Mises ellipse, $\tau_0(\theta)$, and a $m(\theta)$ satisfying (41) and reflecting trends reported by Stout and Hecker for brass

of stress and strain with arbitrary differential hardening have been treated by Hill (1991). Here we are concerned solely with the deformations that accompany stress paths at constant θ. Then (27) simplifies to

$$d\epsilon_1/\cos(\theta-\psi) = d\epsilon_2/\sin(\theta-\psi) = d\gamma/\cos\psi \tag{28}$$

after the substitutions $(\sigma_1,\sigma_2) = \tau(\cos\theta,\sin\theta)$ and $d\gamma = (\sigma/\tau)d\epsilon$. In a case such as (13), the integration starts from a reference locus where $\gamma_0(\theta)$ is known empirically as part of the global representation of radial test data.

The angle ψ varies along a ray in stress space unless successive loci happen to be self-similar. Consequently the associated path in strain space is generally curved. The precise dependence of its curvature on the local geometry and current stress can be seen in Hill (1991, Eq. (4.17)). Typical paths will be exhibited later for values of θ in $(0, \pi/2)$. At this stage we make only a qualitative observation. It is that a strain path may eventually bend so far as to become parallel, momentarily, to one or other orthotropic axis. That is,

$$d\epsilon_1 = 0 \quad \text{when} \quad \psi = \theta - \frac{1}{2}\pi; \text{ or } d\epsilon_2 = 0 \quad \text{when} \quad \psi = \theta. \tag{29}$$

In the presence of differential hardening, therefore, an increment of strain can be plane even when both components of the accumulated strain are positive. As remarked by Hill (1991, pp. 295 and 303), this offers a natural way to account for at least some of the failures by localized necking which often terminate strain paths in the positive quadrants of forming limit diagrams.

Finally we record an elementary formula for future reference. The total differential of τ is expressible as

$$d\tau/\tau = \tan\psi d\theta + \rho d\sigma/\sigma \tag{30}$$

when a family of loci is parameterized by σ. The coefficient ρ here was introduced by Hill (1991) as a convenient measure of the local departure from geometric similarity. It is defined by

$$\rho = (\sigma d\tau)/(\tau d\sigma) \tag{31}$$

where $d\tau$ and $\sqrt{2}\, d\sigma$ here are specifically the radial distance between a pair of neighboring loci in the directions θ and $\pi/4$, respectively; correspondingly $d\tau/\tau$ and $d\sigma/\sigma$ are the proportionate increases in the radii. As an example

$$\rho = \frac{m}{n}\left(\frac{\sigma}{\sigma_0}\right)^{(1+n)/n} \Big/ \left(\frac{\tau}{\tau_0}\right)^{(1+m)/m} \tag{32}$$

for the family (24). Along a reference locus, in particular, ρ is equal to m/n simply; this can be compared with $(1 + n)m/(1 + m)n$ for the family (25).

5 Implementation and Examples

Two procedures for generating families of nonsimilar yield loci were proposed in Section 3. Their implementation is now illustrated in detail by examples for the power law (13). The method would be similar for the alternative law (19) and is readily extended to any other type of hardening.

Procedure (i). Inner and outer loci, $\tau_0(\theta)$ and $\tau_\infty(\theta)$, are specified together with a value of the exponent n for equibiaxial tension. The exponents $m(\theta)$ for loading along any other ray are then calculated by substituting $\tau_\infty(\theta)$ for τ in (24). It is reiterated that this equation is dependent on the hypothesis that converts (15) to (17). Intermediate loci can now be generated at will from (24) as it stands. Precisely the same steps could be followed in relation to (25) when the hypothesis leading to (18) is more appropriate.

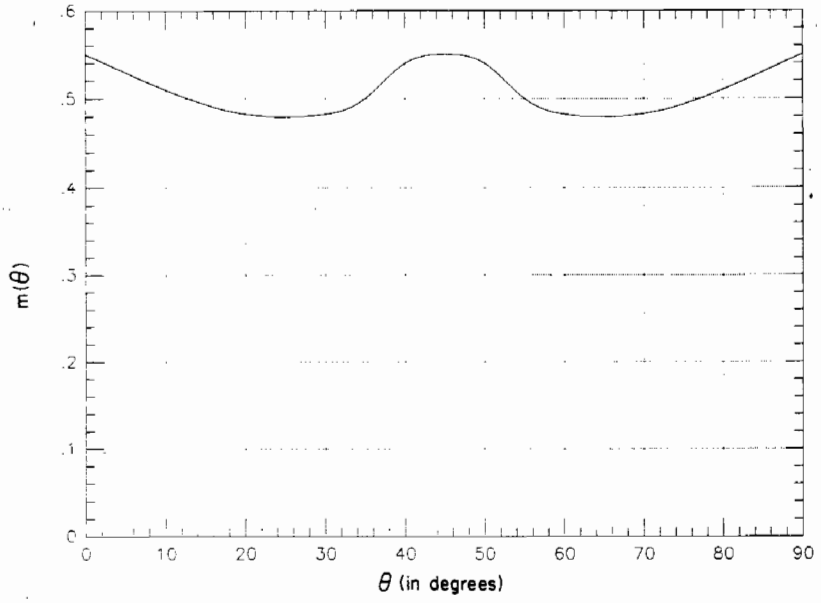

Fig. 7(a)

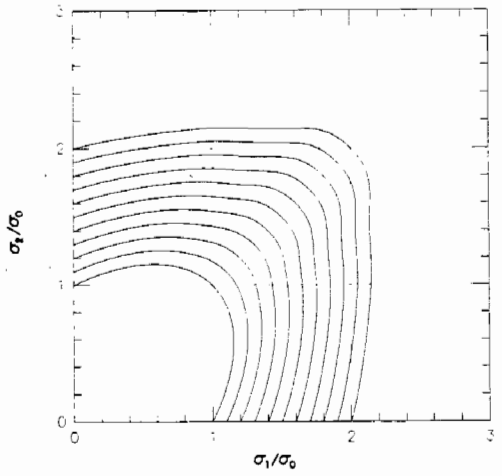

Fig. 7(b)

Fig. 7 An example of $m(\theta)$ which results in non-convex loci. This was one of the iterative variations used in arriving at Fig. 6.

Procedure (ii). An inner locus $\tau_0(\theta)$ is specified together with a predetermined function $m(\theta)$ in $(0, \pi/2)$. This includes the value of n at $\theta = \pi/4$. Exterior loci $\tau(\theta)$ through any designated values of σ/σ_0 can be generated directly from (24) or (25) according to choice.

Procedure (i) will be illustrated by taking the inner and outer loci to be ellipses in (σ_1,σ_2) space. In terms of the standard parameters F, G, H (e.g., Hill, 1990) their equations are

$$(G+H)\sigma_1^2 - 2H\sigma_1\sigma_2 + (F+H)\sigma_2^2 = 1, \tag{33}$$

where the values of F, G, and H are subject to $F + G = 1/\sigma^2 > 0$ and $FG + GH + HF > 0$. Correspondingly

$$\tau(\theta) = [(G+H)\cos^2\theta - 2H \sin\theta \cos\theta + (F+H)\sin^2\theta]^{-1/2}. \tag{34}$$

Suppose, for instance, that the as-received state is characterized by in-plane isotropy (alternatively called normal anisotropy). This necessarily also characterizes the idealized single infinity of loci associated with radial loadings. Therefore $F = G$ for both ellipses; for simplicity we further set $F = H$ on the inner one. The outer ellipse is arbitrarily required to pass through the point $\sigma_1 = \sigma_2 = \sigma_\infty = 2\sigma_0$, and five representative aspect ratios are considered. These are such that

$$H/F = 1/2, 3/5, 1, 5/3, 3.$$

In Fig. 2(*a*) the corresponding loci are labeled A, B, C, D, E in the same order. C is just another Mises ellipse, so in that case the intermediate loci are geometrically similar and $m(\theta) \equiv n$. With the value of n set at 0.3 in all cases, the respective functions $m(\theta)$ resulting from (24) are shown in Fig. 2(*b*). Intermediate members of the corresponding families are shown in Fig. 3(*a*) for case A and in Fig. 4(*a*) for case E. The associated strain paths under various radial loadings are shown in Fig. 3(*b*) and Fig. 4(*b*), respectively. They were computed with (13) rewritten as

$$\tau(\theta) = \tau_0(\theta)\{\gamma(\theta)/\gamma_0(\theta)\}^{m(\theta)}, \quad \gamma(\theta) \geq \gamma_0(\theta). \tag{35}$$

Here $\gamma_0(\theta)$ is defined in relation to $\tau_0(\theta)$ by

$$\tau_0(\theta)\gamma_0(\theta) = \sigma_0\epsilon_0 \tag{36}$$

as explained before, where

$$\sigma = \sigma_0(\epsilon/\epsilon_0)^n \tag{37}$$

under equibiaxial tension. The strain components are computed incrementally by means of (26) and (28). Starting values at the inner locus are assumed to have developed proportionally and are hence given by (28) with ϵ_1, ϵ_2 and $\gamma_0(\theta)$ in place of $d\epsilon_1$, $d\epsilon_2$, and $d\gamma$. On the inner Mises ellipse the values of τ and ψ are given by

$$\tau_0(\theta) = \sigma_0(1 - \sin\theta\cos\theta)^{-1/2},$$

$$\tan\psi_0 = \frac{1}{2}\cos 2\theta/(1 - \sin\theta\cos\theta). \tag{38}$$

The strain paths for case A in Fig. 3(*b*) correspond to loadings along radial rays in $(0, \pi/2)$ at equal intervals, whereas those for case E in Fig. 4(*b*) correspond to rays in $(\theta^*, \pi/4)$ at equal intervals where $\tan\theta^* = 1/2$ (i.e., $d\epsilon_2 = 0$ initially). Note that all paths are curved except under equibiaxial tension. Moreover they bend to an extent such that the criterion (29) for incremental plane strain is eventually met (namely at stages indicated by the solid dots).

To illustrate procedure (ii) we again assume in-plane isotropy and take a Mises ellipse as the inner locus $\tau_0(\theta)$. Consistent with symmetry about $\theta = \pi/4$ and with periodicity π in θ, we chose

$$m(\theta) = m_0 + m_1 \cos\left\{2\left(\theta - \frac{1}{4}\pi\right)\right\} + m_2 \cos\left\{4\left(\theta - \frac{1}{4}\pi\right)\right\} \quad (39)$$

and consider three cases A, B, C (Fig. 5(*a*)) in which the constants m_0, m_1, m_2 are disposed so that

$$\left.\begin{aligned} &\text{A: } m(0)=0.55, \quad m(\theta^*)=0.50, \quad m\left(\frac{1}{4}\pi\right)=0.45;\\ &\text{B: } m(0)=0.45, \quad m(\theta^*)=0.40, \quad m\left(\frac{1}{4}\pi\right)=0.35;\\ &\text{C: } m(0)=0.35, \quad m(\theta^*)=0.30, \quad m\left(\frac{1}{4}\pi\right)=0.25. \end{aligned}\right\} \quad (40)$$

Here, $\tan\theta^* = 1/2$ as before. These choices reflect qualitative trends in the hardening exponents for an aluminum alloy investigated by Wagoner (1980, p. 170); this material was confirmed to retain in-plane isotropy up to strains of order 0.2.

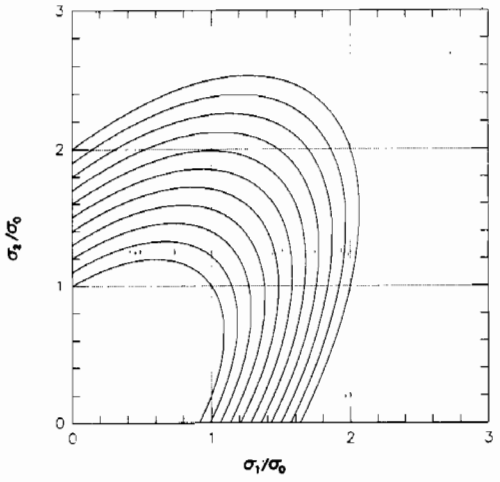

Fig. 8(*a*)

The subsequent loci computed by (24) are shown in Fig. 5(*b*). Probably by chance, some of these are broadly similar in shape to ones constructed by Wagoner (1980, Fig. 8) from an entirely different standpoint. In particular, he predetermined their geometry to conform with the simplest version of Hill's (1979) general yield function. Further, a parameter in this version was varied with strain so that each curve passed through two points determined by experiment: namely a uniaxial yield stress and another inferred from a test in quasi-plane strain (the pair being associated by equal expenditure of work). The respective approaches thus have little or nothing in common, so we have not troubled to simulate another characteristic of this particular aluminum.[1] We are in fact primarily concerned here (and to understand in general terms) how the change in shape of successive loci depends on the magnitude and type of fluctuations in the function $m(\theta)$.

The next example of procedure (ii) was motivated by nonuniformity of the hardening exponent in 70/30 brass as reported by Stout and Hecker (1983). Because of various uncertainties we aim only at qualitative simulation and accordingly impose the constraints

$$m(0)=0.55, \quad m(\theta^*)=0.48, \quad m\left(\frac{1}{4}\pi\right)=0.55. \quad (41)$$

With a Mises inner locus and the representation (39) we found that the resulting yield loci began to develop concavities when σ/σ_0 exceeded 1.5 or so (plots not shown). This phenomenon was still encountered when two more terms with disposable coefficients were added to (39). A different type of representation was therefore tried: values of m were specified at seven points within the interval $(0, \pi/4)$, including those in (41) enforcing symmetry about $\theta = \pi/4$. Interpolation was by cubic splines. By iterating the disposable values we eventually achieved convexity with $m(\theta)$ in Fig. 6(*a*). Some members of the associated family are depicted in Fig. 6(*b*). For comparison, a typical $m(\theta)$ at an intermediate stage of the iteration is given in Fig. 7(*a*). It is seen from Fig. 7(*b*) that a slight concavity has developed in some associated loci. A relatively small variation in $m(\theta)$ was enough to produce this effect. We are inclined to believe that the a priori values stipulated in (41) are

[1]The strain ratio under uniaxial tension did not vary; here this would entail constant ψ and $m'(\theta) = 0$ when $\theta = 0$ and $\pi/2$.

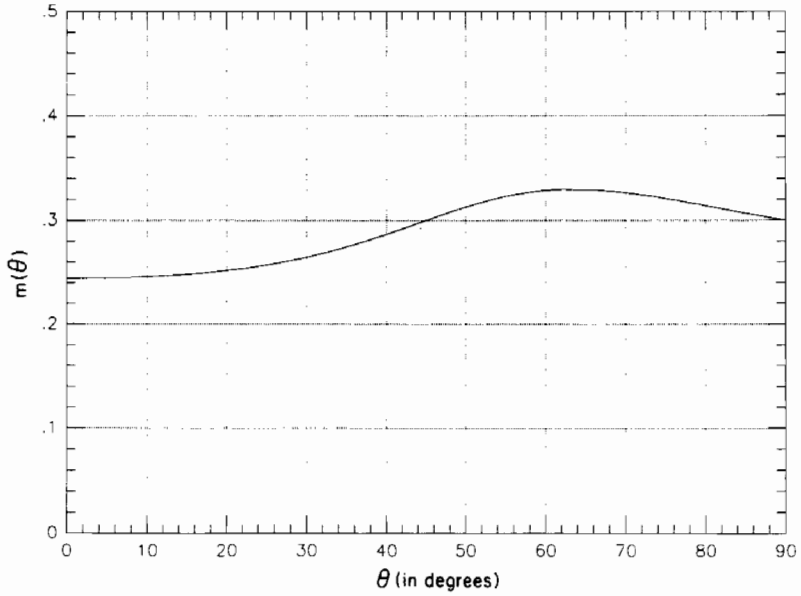

Fig. 8(*b*)

Fig. 8 An example with in-plane orthotropy. The inner locus in an ellipse with $G = H$ and $F/G = 2/3$ and the outer locus is an ellipse with $G = H$ and $F/G = 1/3$; $n = 0.3$ and $\sigma_\infty/\sigma_0 = 2$.

on the edge of possibilities consistent with convexity over the range $1 \le \sigma/\sigma_0 \le 2$. For instance we could not achieve this with any function $m(\theta)$ whatsoever when its value at θ^* was set at 0.45 without changing the others in (41).

In the preceding examples the material was considered to be isotropic in the plane of symmetry; correspondingly its yield function was written as $\phi(\tau,\theta)$, a symmetric function of σ_1 and σ_2 alone. Isotropy was not invoked in full, however, as the biaxial stresses were not oriented arbitrarily within the material but always in the same two directions. In that context the material could alternatively be considered to be one with a special kind of orthotropy. To express this formally, let the yield function be written as $\Phi(\tau,\theta,\alpha)$ where α is the arbitrary angle which σ_1 and σ_2 make with the respective axes of orthotropy. For our purpose the precise dependence on α can be left open; some possibilities have been formulated by Hill (1990). Here we require the function Φ to be special only in that $\Phi(\tau,\theta,0)$ is identified with $\phi(\tau,\theta)$ and is hence likewise symmetric with respect to interchange of σ_1 and σ_2 (equivalent to replacement of θ by $\pi/2 - \theta$). Even though the loci change shape with deformation, this symmetry persists because they are generated as an idealized single infinity from the data in tests where σ_1 and σ_2 are maintained in fixed ratio.

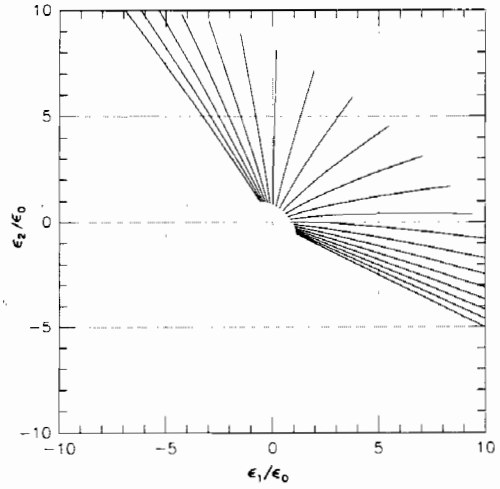

Fig. 9(*a*)

In our next example there is no symmetry of that kind and $\phi(\tau,\theta) \ne \phi(\tau, \pi/2 - \theta)$ in the as-received state. Such a function is incompatible with isotropy and can only be associated with orthotropy in the general sense. Procedure (i) will be adopted in connection with inner and outer ellipses in the family (33) with $F \ne G$. Correspondingly an outward normal is inclined to the local radius at a clockwise angle ψ given by

$$\tan\psi = \{H + (G-F)\tan\theta - H\tan^2\theta\}/\{(G+H) - 2H\tan\theta + (F+H)\tan^2\theta\} \quad (42)$$

from (26). We choose $G = H$ on both ellipses, which has the effect that $\sigma_2 = \sigma$ when $\sigma_1 = 0$ (σ denotes the yield stress in equibiaxial tension). Moreover $\tan\psi = 1/2$ on both when $\theta = 0$, regardless of the value of F/H. There are further consequences under the assumptions (17) and (24). Thus $m(\theta) = n$ on any ray where $\tau_\infty(\theta)/\tau_0(\theta) = \sigma_\infty/\sigma_0$; this happens when $\theta = \pi/2$ if $G = H$. Also $m'(\theta) = 0$ on any ray that meets both ellipses at the same angle; it is easy to verify from (17) and (26) that the ray necessarily meets all intervening loci at a constant angle. By (42) there are two such rays (conjugate with respect to each ellipse), namely $\theta = 0$ deg where $\sigma_2 = 0$ and $\psi = \tan^{-1} 1/2 = 26.565$ deg, and $\theta = \tan^{-1} 2 = 63.435$ deg where $\sigma_2 = 2\sigma_1$ and $\psi = -\tan^{-1} 1/2$. Both values of ψ are unaffected by the ratio F/G when $G = H$. Furthermore the incremental strain is plane ($d\epsilon_1 = 0$) on the latter ray, and so the associated strain path is linear ($\epsilon_1 = 0$). All these features are seen in Fig. 8(*a*), (*b*) which show $m(\theta)$ and the family of loci when $n = 0.3$ and F/G is chosen to be 2/3 on the inner ellipse and 1/3 on the outer one through $\sigma_\infty/\sigma_0 = 1$ and 2, respectively. Their major axes are inclined to the σ_1 axis at angles 49.7 deg and 54.2 deg, respectively. Representative strain paths are shown in Fig. 9(*a*) for rays equally spaced between $\theta = 0$ and $\pi/2$, and in Fig. 9(*b*) for rays equally spaced between $\theta = \theta^*$ and $\pi/4$, where now $\theta^* = 30.7$ deg at the point where $d\epsilon_2 = 0$ on the inner ellipse. Points where the incremental strain is plane are indicated by solid dots.

We conclude with some practical observations regarding the computing technique. With procedure (i) any convex curves could be considered for $\tau_0(\theta)$ and $\tau_\infty(\theta)$ (and not just ellipses). Values of these functions can be prescribed on selected rays and then interpolated by splines or an appropriate alternative. The values of m can likewise be computed on arbitrarily selected rays; we chose to space these equally but as closely as

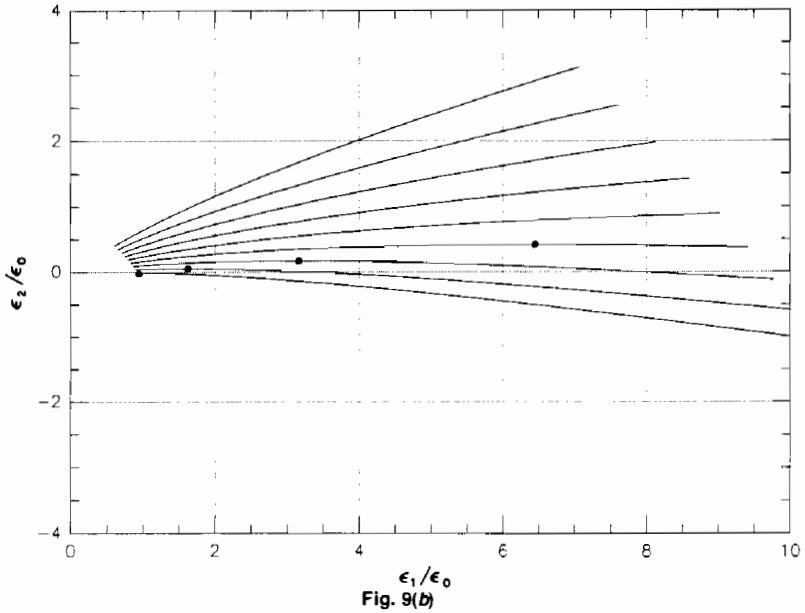

Fig. 9(*b*)

Fig. 9 Strain trajectories under radial stress loading for the family of loci shown in Fig. 8

required. In procedure (ii), $m(\theta)$ has to be prescribed in advance; we used either cubic splines or formula (39) to represent this function. The former was found very effective when checking convexity, as interpolation could be based on relatively few values of m. In both procedures the angle ψ has to be determined by computing $m'(\theta)$. Several methods could be adopted, depending on how $m(\theta)$ is represented; for convenience we always used the simplest approximation: namely $[m(\theta + \delta) - m(\theta - \delta)]/2\delta$.

6 Closing Remarks

The preceding analysis is concerned with the plastic response of isotropic or orthotropic sheet under biaxial loading, more especially when the shape of successive yield loci varies. This is an expected consequence of changes in crystalline texture during continued deformation. As often remarked in regard to the normality flow rule, relatively small variations in shape can significantly affect the cumulative strains associated with a given stress path. On that account among others, experimental determinations of successive loci over a finite range of strain are a prerequisite for any useful theory. Such tests are technically demanding, and the area to be explored is extensive. With this in mind, we have devised a simple analytical framework in the hope that it may contribute to the design of future tests and sharpen the perceived objectives.

Aside from admitting families of nonsimilar yield loci, the constitutive basis is broadly classical. For the present we see no advantage in relaxing any other element in that description. We have, in particular, retained the customary fiction that the totality of potential loci is singly infinite, nonintersecting, and parameterized by the work expended. The idealization is plainly unrealistic in detail, for instance by virtue of the path dependence mentioned at the outset.

It must be regarded, therefore, as a pragmatic expedient until such time as it can be confronted by quantifiable data. Meantime some minor improvements are feasible and should be considered. Representation of radial tests by the power law (13) is not obligatory, and it is conceivable that (19) would be more apt for some materials in their as-received states. More generally, contours $\tau(\theta,w_1)$, $\tau(\theta,w_2)$, ... of equal work at discrete values of w could just as easily be constructed from any kind of representation $\tau(w,\theta_1)$, $\tau(w,\theta_2)$, ... of the radial test characteristics at discrete values of θ. A basic question remains: to what extent, and in what circumstances, is it realistic for contours of equal work to act as yield loci in the limited sense of determining normals for the classical flow rule?

Acknowledgment

The work of JWH was supported in part by the National Science Foundation under Grant MSM-88-12779, and in part by the Division of Applied Sciences, Harvard University.

References

Chan, K. C., and Lee, W. B., 1990, "A Theoretical Prediction of the Strain Path of Anisotropic Sheet Metal Deformed under Uniaxial and Biaxial Stress State," *Int. J. Mech. Sci.*, Vol. 32, pp. 497–511.

Ghosh, A. K., and Backofen, W. A., 1973, "Strain Hardening and Instability in Biaxially Stretched Sheets," *Metall. Trans.*, Vol. 4, pp. 1113–1123.

Ghosh, A. K., 1978, "Plastic Flow Properties in Relation to Localized Necking in Sheets," *Mechanics of Sheet Metal Forming, Material Behavior and Deformation Analysis*, D. P. Koistinen and N.-M. Wang, eds., Plenum Press, New York.

Hill, R., 1979, "Theoretical Plasticity of Textured Aggregates," *Proc. Cambridge Philos. Soc.*, Vol. 85, pp. 179–191.

Hill, R., 1990, "Constitutive Modelling of Orthotropic Plasticity in Sheet Metals," *J. Mech. Phys. Solids*, Vol. 38, pp. 405–417.

Hill, R., 1991, "A Theoretical Perspective on In-plane Forming of Sheet Metal," *J. Mech. Phys. Solids*, Vol. 39, pp. 295–307.

Lequeu, P. H., and Jonas, J. J., 1988, "Modelling of the Plastic Anisotropy of Textured Sheet," *Metall. Trans.*, Vol. 19A, pp. 105–120.

Stout, M. G., Hecker, S. S., and Bourcier, R., 1983, "An Evaluation of Anisotropic Effective Stress-Strain Criteria for the Biaxial Yield and Flow of 2024 Aluminum Tubes," ASME *Journal of Engineering and Materials Technology*, Vol. 105, pp. 242–249.

Stout, M. G., and Hecker, S. S., 1983, "Role of Geometry in Plastic Instability and Fracture of Tubes and Sheet," *Mech. Mat.*, Vol. 2, pp. 23–31.

Stout, M. G., and Staudhammer, K. P., 1984, "Biaxial Deformation of 70-30 Brass: Flow Behaviors, Texture, Microstructures," *Metall. Trans.*, Vol. 15A, pp. 1607–1612.

Wagoner, R. H., 1980, "Measurement and Analysis of Plane-Strain Work Hardening," *Metall. Trans.*, Vol. 11A, pp. 165–175.

Wagoner, R. H., 1982, "Plastic Behavior of 70/30 Brass Sheet," *Metall. Trans.*, Vol. 13A, pp. 1481–1500.